Received 25 July 2007
Revised 17 March 2008
Accepted 7 April 2008

Flow simulation in a complex fluidics using three turbulence models and unstructured grids

Junye Wang
North Wyke Research, Okehampton, UK, and
Geoffrey H. Priestman
Department of Chemical and Process Engineering, The University of Sheffield, Sheffield, UK

Abstract

Purpose – The purpose of this paper is to simulate the behaviour of the symmetrical turn-up vortex amplifier (STuVA) to obtain insight into its maximum through-flow operation within the eight-port STuVA, and understand the relation between its design parameters and flow characteristics. Furthermore, it is to test the performance of different turbulent models and near-wall models using the same grid, the same numerical methods and the same computational fluid dynamics code under multiple impingement conditions.

Design/methodology/approach – Three turbulence models, the standard k-ε, the renormalization group (RNG) k-ε model and the Reynolds stress model (RSM), and three near-wall models have been used to simulate the confined incompressible turbulent flow in an eight-port STuVA using unstructured meshes. The STuVA is a special symmetrical design of turn-up vortex amplifier, and the simulation focused on its extreme operation in the maximum flow state with no swirling. The predictions were compared with basic pressure-drop flow rate measurements made using air at ambient conditions. The effect of different combinations of turbulence and near-wall models was evaluated.

Findings – The RSM gave predictions slightly closer to the experimental data than the other models, although the RNG k-ε model predicted nearly as accurately as the RSM. They both improved errors by about 3 per cent compared to the standard k-ε model but took a long time for convergence. The modelling of complex flows depends not only on the turbulence model but also on the near-wall treatments and computational economy. In this study a good combination was the RSM, the two layer wall model and the higher order discretization scheme, which improved accuracy by more than 10 per cent compared to the standard k-ε model, the standard wall function and first order upwind.

Research limitation/implications – The results of this paper are valid for the global pressure drop flow rate. It should be desirable to compare some local information with the experiment.

Originality/value – This paper provides insight into the maximum through-flow operation within the eight-port STuVA to understand the relation between its design parameters and flow characteristics and study the performance of turbulence and near wall models.

Keywords Fluidics, Turbulence, Numerical analysis, Simulation
Paper type Research paper

Nomenclature

C_μ, C_1, C_2, $C_{1\varepsilon}$, $C_{2\varepsilon}$, C_3	constants in turbulence model	Up	mean velocity of the fluid at point p
k	turbulent kinetic energy (m^2/s^2)	$\rho\,\overline{u_i' u_j'}$	Reynolds stress
		x_i, x_j	coordinate
Pr_t	Prandtl number for energy	y	the normal distance from the wall at the cell centres
u_i	mean velocity in direction x_i (m/s)		
u_j	mean velocity in direction x_j	y_v	physical viscous sub-layer

International Journal of Numerical Methods for Heat & Fluid Flow
Vol. 19 Nos. 3/4, 2009
pp. 484-500

0961-5539
DOI 10.1108/09615530910938399

Greek letters

α inverse effective Prandtl number

β coefficient of thermal expansion

ε turbulent dissipation rate (m^2/s^3)

η Sk/ε

μ viscosity (Pa s)

μ_t turbulent viscosity (defined by Equation (3))

μ_{eff} effective visicosity

ρ density (kg/m^3)

$\sigma_k, \sigma_\varepsilon$ constants

δ_{ij} Kronecker symbol, $\delta_{ij} = 1$ if $i = j$ and $\delta_{ij} = 0$ if $i \neq j$

Ω rotation vector

1. Introduction

The vortex amplifier is a generic fluidic component in which the passage of flow through a vortex chamber between a tangential supply and an axial outlet can be modulated by the introduction of a control flow at the chamber periphery. It has been used in many varied applications ranging from ventilation flow control to flow measurement (Priestman and Tippetts, 1984; Wang *et al.*, 1997). Turn-up vortex amplifier (TuVA) is one of various fluidics vortex amplifiers in which the supply and the control flow both enter the chamber periphery tangentially, but in opposition. Thus the introduction of control flow tends to oppose the vortex created by the supply flow, with the result that the through-flow is increased or "turned-up". The control inlet is normally relatively small, such that a relatively high pressure but low flow control stream modulates a much larger but lower pressure supply flow. Symmetrical turn-up vortex amplifier (STuVA) is a special design of TuVA in which the control and supply ports are identical to each other, giving symmetry to the device. The STuVA has unique and complex own characteristics. A common pressure supplied to the control and supply ports give a maximum through-flow with, in theory, no vortex, whilst a minimum through-flow and maximum vortex strength is achieved if flow only enters through one of the inlet ports. These special characteristics enable the STuVA to be applied as a level control in pressurised vessels, such as oil–gas production separators (Priestman and Tippetts, 1998, 2000).

The application of vortex amplifiers often requires special consideration to its system stability. Instabilities can occur both due to the properties of the characteristics of the vortex amplifier alone or from its interaction with the resistive or capacitive characteristics of associated pipe-work or vessels. The unique design of the STuVA produced particular instability problems. It was found that a basic two inlet port STuVA exhibited an internal flow instability when applied in a level control system (Priestman and Tippetts, 2000). The problem was found to be associated with an inability of the device to establish a completely vortex free flow state in the maximum flow condition. That is inflow through two identical opposed inlets from a common pressure source did not produce stable symmetrical inflows. Two stable states were possible, each with one of the inlets dominating the flow. The instability significantly reduced the overall performance of the level controller, and also resulted in flow oscillations for some pipework configurations. It was found, however, that the problem could be avoided if the supply and control flows were divided between multiple chamber inlets, as illustrated in the eight-port STuVA design shown in Figure 1. Although redesigning the STuVA has apparently removed the instability, an understanding of the internal flows producing it is still required.

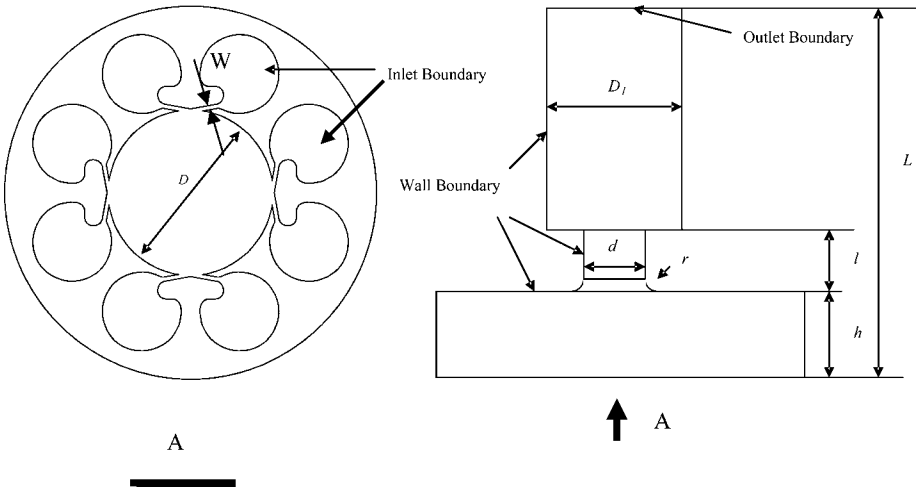

Figure 1.
Design and boundary conditions for the STuVA

A key issue in such simulation is the modelling of turbulence and the near wall region. Many workers have focussed on turbulence models. Thakur *et al.* (1996) evaluated the different modifications to the basic two-equation k-ε model, which took the non-equilibrium between the production and dissipation of k and ε and rotational effects into account. Younis *et al.* (1996) evaluated algebraic stress models. Menter (1996) compared the standard k-ε model and the renormalization group (RNG) k-ε models. Guo *et al.* (2001) evaluated four turbulence models (the standard k-ε model, the RNG k-ε model, low Reynolds number k-ε model and the Reynolds stress model (RSM)) applied to the simulation of a two-dimensional submerged jet. Based on comparison between the observed and predicted behaviour of the oscillation, as well as the computational economy, they recommended the k-ε model for the confined jet. Sarkar *et al.* (1997) compared three different versions of high-Re k-ε models of turbulence for simulation of flow past the entire length of axisymmetric bodies. They found that the simple standard k-ε model with wall functions presents the flow characteristics past axisymmetric bodies at least as accurately as the more complicated RNG models. It should be noted, however, that the above studies were based on relatively simple geometries using structured meshes. Furthermore, the significance of the near-wall treatments were not taken into account at the above work.

Turbulent flows are significantly affected by the presence of walls. It is in the near wall region that the solution variables change with large gradients, and the momentum and other scalar transports occur most vigorously. Therefore, the turbulent models must be suitable for the wall-bounded flows. Many near-wall treatments have been developed as an extension of turbulence model closure to fit low Reynolds number flows and to describe the flow close to a solid wall (Johston and Flack, 1996; Patel *et al.*, 1985).

An early simulation of flow in a basic vortex throttle was done by Yang *et al.* (1991) using the two-equation k-ε model and RSM. More recently, Woolhouse *et al.* (2000) simulated flows within a basic TuVA. However, the complex geometry of the present eight-port STuVA makes the simulation more challenging. The eight-port STuVA operation states are very complicated, but its performance is mainly determined by its two extreme operating states: a minimum through-flow with strongly swirling vortex

and a maximum through-flow with non-swirling and multiple impingement flow. Doubt remains, of the ability of these approaches to model our complex system due to reliance of turbulence models on some empirical information. Wang *et al.* (2006) modelled one of its two extreme operating states: a minimum through-flow with strongly swirling vortex. It was found that the standard two-equation k-ε and RSM models were deviated from experimental data. This is in agreement with other researches of the swirling flows (Slack *et al.*, 2000; He *et al.*, 1999; Malhotra *et al.*, 1994). The model constants must be adjusted for the strongly swirling flows.

However, no attempts have done for another extreme operating state, the maximum through-flow state. This operating state includes more complex multiple impingement flows. Every two opposite jets from the inlets impinge each other and form one new jet. The four new jets impinge at centre of the vortex chamber and flow into a nozzle. As mentioned before, the instability problem was mainly associated with this maximum through-flow state to establish a completely vortex free flow state in the two port TuVA. That is inflow through two identical opposed inlets from a common pressure source did not produce stable symmetrical inflows. Hence, it is necessary to simulate this extreme operating state for further understanding of complex impingement flow within the STuVA.

This paper aims to simulate the flow field of the STuVA using computational fluid dynamics (CFD) to obtain some insight into its maximum through-flow operation within the eight-port STuVA, and to understand the relation between its design parameters and flow characteristics. While Wang *et al.* (2006) studied an extreme operating state, minimum through-flow with strongly swirling vortex, this paper concentrates on another extreme operating state, the maximum through-flow with multiple impingements and no vortex when all the inlets are subject to a common pressure and ideally little or no vortex is formed in the chamber. Through that a better understanding of the complicated flow field can be achieved and possibly enable improved design of the device. Another aim is to test the performance of different turbulent models and near-wall models using the same grid, the same numerical methods and the same CFD code under multiple impingement conditions. In the next section, the experimental facility is briefly introduced.

2. Experimental characterisation of the STuVA

A previously optimised (Priestman and Tippetts, 2000) design of eight-port STuVA was characterised to provide basic data for comparison with the model predictions. The STuVA geometry is illustrated in Figure 1 with Table I giving details of the critical dimensions in millimetres. The axial outlet nozzle was made of brass and its 13 mm diameter section was 20 mm long. The inlet ports were 2.35 mm wide across the full chamber height.

A schematic drawing of the experimental rig is shown in Figure 2. A fan was used to draw air through the device from atmosphere. The pressure drop was measured using an inclined manometer on the downstream developed turbulent region of the outlet nozzle. Pressure drop was limited to less than 20 cm of water to avoid

D (mm)	D_1 (mm)	D (mm)	H (mm)	L (mm)	L (mm)	R (mm)	W (mm)
90	50	13	29.1	20	149.1	4	2.23

Table I.
Dimensions and parameters of the eight-port STuVA

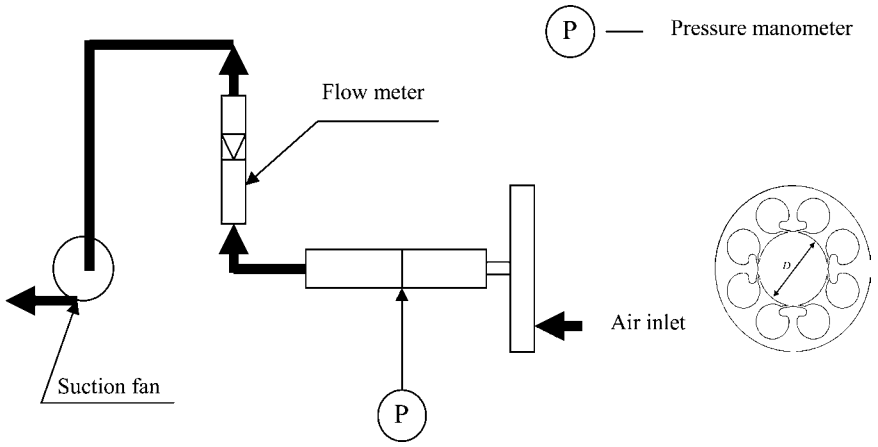

Figure 2.
Schematic of experimental system

compressibility effects. Furthermore, since the air was draw from atmosphere through the inlets and the flow performance is only related to not the local pressure at the inlet and outlet but the pressure difference between the inlet and outlet. An inclined manometer is for the measurement of the outlet pressure, and no pressure senor is required for the inlet since the inlet pressure is at atmosphere ones. A rotameter positioned downstream of the outlet pressure tapping measured the flow rate, readings being adjusted for density. Pressure drop was measured to ±10 Pa. The rotameter accuracy was about ±2 per cent.

3. Outline of turbulence models

Three widely applied turbulence models, the standard k-ε model, the RNG k-ε model and the RSM have been used. Only the essential features of these turbulence models are presented, details being available elsewhere (Versteeg and Malalasekera, 1995; Ferziger and Peric, 1999; FLUENT Incorporated, online version).

3.1 The standard two-equation k-ε model

The turbulent kinetic energy k and its dissipation rate ε are calculated from the following transport equations:

$$\rho\frac{Dk}{Dt}=\frac{\partial}{\partial x_i}\left(\left[\mu+\frac{\mu_t}{\sigma_k}\right]\frac{\partial k}{\partial x_i}\right)-\rho\overline{u_i'u_j'}\frac{\partial u_j}{\partial x_i}+\beta g_i\frac{\mu_t}{\mathrm{Pr}_t}\frac{\partial T}{\partial x_i}-\rho\varepsilon-2\rho\varepsilon\frac{k}{\gamma RT} \quad (1)$$

$$\rho\frac{D\varepsilon}{Dt}=\frac{\partial}{\partial x_i}\left(\left[\mu+\frac{\mu_t}{\sigma_\varepsilon}\right]\frac{\partial \varepsilon}{\partial x_i}\right)+C_1\frac{\varepsilon}{k}\left(-\rho\overline{u_i'u_j'}\frac{\partial u_j}{\partial x_i}+C_3\beta g_i\frac{\mu_t}{\mathrm{Pr}_t}\frac{\partial T}{\partial x_i}\right)-C_2\rho\frac{\varepsilon^2}{k} \quad (2)$$

The turbulent viscosity is related to k and ε by:

$$\mu_t=\rho C_\mu\frac{k^2}{\varepsilon} \quad (3)$$

The above equations contain six adjustable coefficients C_μ, C_1, C_2, C_3, σ_k and σ_ε. The standard values of the model coefficients in the standard k-ε model are 0.09, 1.44, 1.92, 2.0, 1.0 and 1.3, respectively.

3.2 The RNG k-ε model

The RNG k-ε model has a similar form to the standard k-ε model except for their coefficients. Hence, the RNG k-ε model can be solved in exactly the same way as the standard k-ε model. Two main coefficients of Equations (1) and (2) have been modified in the RNG k-ε model of the FLUENT code: the coefficient C_2 in the dissipation term and the eddy viscosity μ_t.

C_2 in Equation (2) is replaced by C_2^*, defined as

$$C_2^* = C_2 + \frac{C_\mu \rho \eta^3 (1 - \eta/\eta_0)}{1 + \beta \eta^3} \tag{4}$$

Where $\eta_0 = 4.38, \eta = Sk/\varepsilon$ and $\beta = 0.012$. The standard values of the RNG k-ε model coefficient are $C_\mu = 0.0845$, $C_1 = 1.42$ and $C_2 = 1.68$. When $\eta < \eta_0$, the correction term in Equation (4) makes a positive contribution, and C_2^* becomes larger than C_2. When $\eta > \eta_0$, the correction term makes a negative contribution, and C_2^* becomes less than C_2.

The eddy viscosity in the RNG k-ε model is replaced with an effective eddy viscosity based on the equation below for low Reynolds number:

$$\mu_t = \sigma(\alpha \mu_{eff} - \mu) \tag{5}$$

Where α is the inverse effective Prandtl number, and μ_{eff} is calculated from the following differential equation which is based on the RNG theory:

$$d\left(\frac{\rho^2 k}{\sqrt{\varepsilon \mu}}\right) = 1.72 \frac{\hat{\nu}}{\sqrt{\hat{\nu}^3 - 1 + C_\nu}} d\hat{\nu} \tag{6}$$

Where $\hat{\nu} = \mu_{eff}/\mu$, $C_v \approx 100$. For high-Reynolds number Equation (6) is reduced to Equation (3).

3.3 Reynolds stress models

The RSM solves seven partial differential equations, six of them for the six independent Reynolds stresses and one for the dissipation of turbulent kinetic energy. The standard RSM can be given as follows

$$\frac{D}{Dt}\left(\rho \overline{u_i' u_j'}\right) = \frac{\partial}{\partial x_k}\left(\frac{\mu_t}{\sigma_k}\frac{\partial \overline{u_i' u_j'}}{\partial x_k}\right) + \frac{\partial}{\partial x_k}\left(\mu \frac{\partial \overline{u_i' u_j'}}{\partial x_k}\right) + P_{ij} + \phi_{ij} - \frac{2}{3}\rho \varepsilon_{ij} \delta_{ij} + F_{ij} \tag{7}$$

where

$$P_{ij} = -\rho\left(\overline{u_i' u_k'}\frac{\partial U_j}{\partial x_k} + \overline{u_j' u_k'}\frac{\partial U_i}{\partial x_k}\right) \tag{8}$$

$$\mu_t = \rho C_\mu \frac{k^2}{\varepsilon} \tag{9}$$

$$\phi_{ij} = -C_1 \rho \frac{\varepsilon}{k}\left(\overline{u_i' u_j'} - \frac{2}{3}k\delta_{ij}\right) - C_2\left(P_{ij} + Fij - \frac{2}{3}P_{ij}\delta_{ij}\right) \tag{10}$$

$$F_{ij} = -2\rho\Omega_k\left(\overline{u_j' u_m'} e_{ikm} + \overline{u_i' u_m'} e_{jkm}\right) \tag{11}$$

Ω_k is the rotation vector and e_{ijk} is the alternating symbol; $e_{ijk} = 1$ if i, j and k are different and in cyclic order, $e_{ijk} = -1$ if i, j and k are different and in anti-cyclic order, and $e_{ijk} = 0$ if any two indices are the same. The transport equation of the scalar dissipation rate ε is identical to Equation (2). The above equations contain seven adjustable constants C_μ, C_1, C_2, $C_{1\varepsilon}$, $C_{2\varepsilon}$, σ_k and σ_ε. The standard values of the model coefficients in the RSM model are 0.09, 1.8, 0.6, 1.44, 1.92, 1.0 and 1.0, respectively.

4. The near wall treatments

The turbulence models are primarily valid for fully developed turbulent flows. Consideration therefore needs to be given of how to make these models suitable for near-wall flows. The common near-wall treatments are wall functions, non-equilibrium wall functions and two layer zonal model.

4.1 Wall functions

The wall functions do not resolve the viscosity affected inner region (viscous sub-layer and buffer layer). Instead, semi-empirical formulas are used to bridge the viscosity-affected region between the wall and the fully-turbulent region. The-law-of-the-wall for mean velocity yields (Launder and Spalding, 1974):

$$U^* = \frac{1}{k}\ln(Ey^*) \tag{12}$$

where

$$U^* = \frac{U_p C_\mu^{1/4} k_p^{1/2}}{\tau_w/\rho} \tag{13}$$

$$y^* = \frac{\rho C_\mu^{1/4} k_p^{1/2} y_p}{\mu} \tag{14}$$

and k (= 0.4187) is the von Karman constant, U_p the mean velocity of the fluid at point p, E (= 9.793) an empirical constant, k_p represents turbulent kinetic energy at point p, and y_p the distance from point p to the wall.

In the FLUENT, when $y^* > 11.225$ the log-law is employed and at the wall-adjacent cells, the laminar stress-strain relationship, $U^* = y^*$.

4.2 Non-equilibrium functions

The non-equilibrium functions assume that the wall-neighbouring cells consist of a viscous sub-layer and a fully turbulent layer and need to resolve the k equation at the wall-neighbouring cells. Thus, the non-equilibrium wall functions partly account for non-equilibrium effects neglected in the standard wall function. The log-law for mean velocity sensitized to pressure gradients is:

$$\frac{\tilde{U} C_\mu^{1/4} k^{1/2}}{\tau_w/\rho} = \frac{1}{k}\ln\left(E\frac{\rho C_\mu^{1/4} k^{1/2} y}{\mu}\right) \tag{15}$$

where

$$\tilde{U} = U - \frac{1}{2}\frac{dp}{dx}\left[\frac{y_v}{\rho k^{3/2}}\ln\left(\frac{y}{y_v}\right) + \frac{y - y_v}{\rho k^{3/2}} + \frac{y_v^2}{\mu}\right] \tag{16}$$

and

$$y_v = \frac{\mu y_v^*}{\rho C_\mu^{1/4} k_p^{1/2}} \tag{17}$$

Where y_v is physical viscous sub-layer thickness, and $y_v^* = 11.225$. Thus the profile assumption made for turbulence quantities are:

$$\tau_w = \begin{cases} 0 & y < y_v \\ \tau_w & y > y_v \end{cases} \tag{18}$$

$$k = \begin{cases} \left(\frac{y}{y_v}\right)^2 k_p & y < y_v \\ k_p & y > y_v \end{cases} \tag{19}$$

$$\varepsilon = \begin{cases} \frac{2\nu k}{y^2} & y < y_v \\ \frac{k^{3/2}}{k C_\mu^{-3/4} y} & y > y_v \end{cases} \tag{20}$$

4.3 Two layer models

The two layer near-wall models divide the whole domain into two regions, a viscosity-affected region and a fully-turbulent region. The turbulent models are modified to enable the viscosity-affected region to be resolved. The two regions are determined by a wall-distance-based turbulent Reynolds number, as $\mathrm{Re}_y = (\rho y\sqrt{k})/\mu$, where y is the normal distance from the wall at the cell centres.

Thus, in the fully developed turbulent region, $\mathrm{Re}_y > \mathrm{Re}_y^*$ and $\mathrm{Re}_y^* = 200$; the turbulence models are employed. In the viscosity-affected near-wall region, $\mathrm{Re}_y < \mathrm{Re}_y^*$; the one-equation model of Wolfstein is employed (Wolfstein, 1969). The momentum equations and the k equation are same as those in the turbulence models. The turbulent viscosity, μ_t, is computed from

$$\mu_{t,2layer} = \rho C_\mu l_\mu \sqrt{k} \tag{21}$$

Where the length scale, l_μ, is calculated from Reference (Chen and Patel, 1988).

5. Numerical considerations

The computer program in the present work was the FLUENT 6. The code is able to accommodate non-uniform and unstructured grids. Tetrahedral unstructured meshes are generated by the GAMBIT 2.2.30, as shown in Figure 3. For successful computation of turbulent flows consideration during the mesh generation is required. In particular, the two layer model needs to resolve the viscosity-affected region. In other words, the mesh in the near-wall region should be locally refined and have enough cells to resolve turbulence quantities. The FLUENT 6 package offers adaptive grid functions. The advantage of the adaptive grid is that the refined grids occupy only a small part of the domain and the total number of grid points is relatively small, so both the cost of

computation and memory requirements are reduced enormously. Here $Y^+ = 1$ was used to regenerate the meshes locally in the near-wall region. Figure 4 shows a locally refined mesh in the near-wall regions. It can be seen that the narrow gaps also were refined due to the refinements of both sidewalls.

Since the governing partial differential equations were elliptic for incompressible viscous flows, it was necessary to define boundary conditions for all variables on all boundaries of the flow domain. Three types of boundary conditions were used, inlet, outlet and wall, as illustrated in Figure 1. The boundaries of the inlets and the outlet were specified to be steady-state. The inlet conditions were known beforehand; therefore, the pressure inlets were pre-set at the beginning of the computation. The outlet condition was not known, and the zero-gradient conditions were applied on the assumption that the flow had become more or less fully developed when it reached the exit plane. At the solid wall, the non-slip condition was applied which meant that the velocity of the fluid at the wall should be the same as that of the wall. Hence, the velocity at the wall was specified to be zero.

The SIMPLE algorithm was used for coupling the pressure and velocity equations. The algorithm was originally put forward by Patankar and Spalding (1972) and was essentially a guess-and-correct procedure for the calculation of pressure on the staggered grid arrangement. All the models were tested using the k-ε model with the same numerical methods and with the same boundary conditions on identical meshes. Two discretization schemes, first order upwind and the quadratic upwind differencing scheme (QUICK), were used for discretization of momentum, turbulence kinetic energy and turbulence dissipation rate. It should be mentioned that FLUENT 6 allows the use of the QUICK scheme for unstructured grids; in such cases the usual second-order upwind discretization scheme are used at the faces of non-hexahedral cells. Hence, the

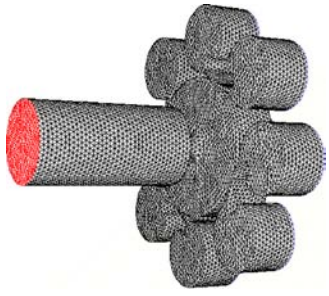

Figure 3.
Illustration of the tetrahedral mesh for the STuVA

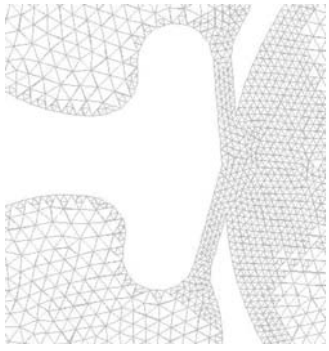

Figure 4.
Locally re-fined cells at the near wall region

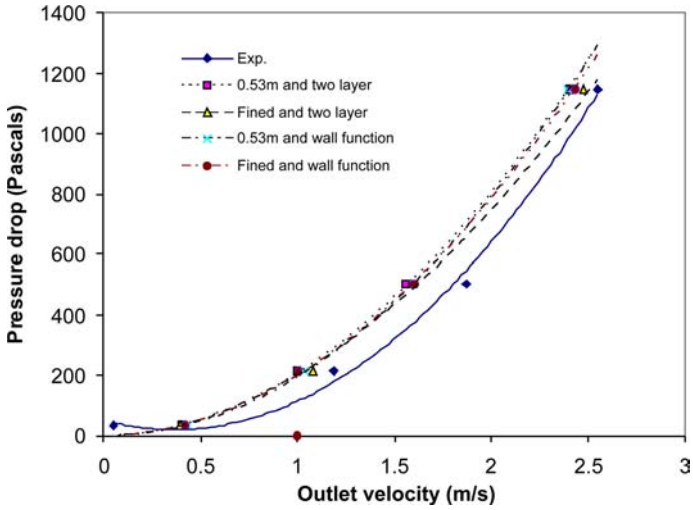

Figure 5.
The effect of grid adaptation and wall treatments on the solution

QUICK scheme is replaced by the second-order upwind scheme for the present unstructured grid.

The grid independent solution was established using four successively refined grids with 0.147, 0.294, 0.533 and 1.23 million cells. The testing showed that the difference of mass flow rates at the outlet was 2.6 per cent between 0.535 and 1.23 million cells under a pressure drop of 36.5 Pa using the first-order upwind scheme and 1.3 per cent using the QUICK scheme. The effect of the adaptive grid on the solutions was also tested using the k-ε model. The computations started using the mesh of 0.535 million cells. Then, the 0.533 million grid was further refined to 0.762 million cells using the Y^+ function after several hundred iterations. It was found that the difference of the mass flow rates from its consecutive grid of 1.23 million cells was 2.4 per cent for the first-order upwind scheme under a pressure drop of 36.5 Pa and 0.7 per cent for the QUICK scheme.

The adaptive refined grid (0.762 million cells) and the 0.533 million cell grid were compared to evaluate the effect of the standard wall function and the two layer model. The testing used the standard k-ε model with the first order upwind. Figure 5 shows that a combination of the adaptive refined grid and the two layer model do improve the solution by between 1 and 3 per cent compared to the other combination. Using the QUICK scheme, the difference of the solution was about 0.5 per cent between the two grids for both the standard wall function and the two layer treatments. It can also be seen that there is a very small difference in using the wall function with the adaptive fined grid and the original 0.533 million cell grid. The refined mesh has not caused substantial errors. This gives us confidence to use the combination of the adaptive fined mesh (0.762 million cells) for subsequent computations.

6. Results and discussion

6.1 Solution procedures

In order to compare the simulations with the data, the boundary conditions were set to a given pressure drop and the predicted flow rate then compared with the measured one. The standard two equation k-ε model was the easiest of the three turbulent models to converge. For the RNG k-ε model lower under-relaxation factors were employed due

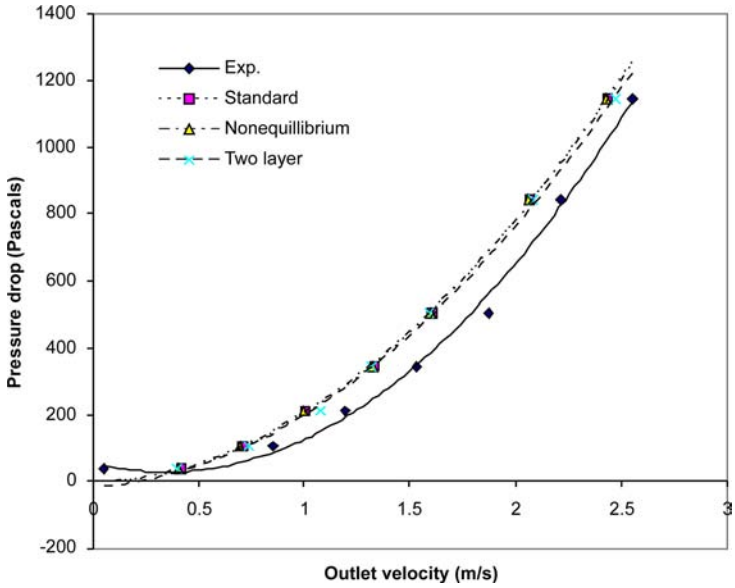

Figure 6.
Comparison of three near wall models: the wall function, non-equilibrium wall function and the two layer model using the standard k-ε with the first order upwind

to convergence difficulty caused by its additional non-linearities. To accelerate convergence the solutions of the standard k-ε model were used for the initial guess of the RNG k-ε model. Then, the standard k-ε model was switched to the RNG k-ε model to continue numerical iterations until the convergence. Likewise, because the RSM creates a high non-linearly coupling between the momentum equations and the turbulent stresses, the computation was more prone to stability and convergence difficulties than those using the k-ε model. Hence, the computation was also started with the standard k-ε model to accelerate convergence, and then switched to the RSM, with low under-relaxation factors being employed to avoid the divergence.

6.2 Comparison of near-wall treatments

Figure 6 shows the effect of the near-wall models on the solutions. Note that the flow rate predicted for each pressure drop is expressed in terms of an average outlet velocity. The turbulence model used was the standard k-ε model with the first order scheme. It can be seen that the predicted pressure drop of all three wall treatments is slightly higher than the experimental data, except for the lowest outlet velocity. Overall, the two layer model shows slightly better agreement with the experimental data, particularly at lower flow rate region. This may be because at lower Reynolds numbers the viscosity-affected near-wall region, in which the solution variables change most slowly, becomes more important and needs to be resolved, particularly for smaller passages. In such flows the turbulence is subjected to severe adverse pressure gradients and changes rapidly, and the wall function approach becomes less reliable. The two layer model can resolve the viscosity-affected region and give a better descriptions for near-wall flow.

6.3 Comparison of turbulence models

Figure 7 shows predictions using the two layer model for the standard two-equation k-ε model and the RNG k-ε model using both the first order scheme and the QUICK scheme. The RNG model with the QUICK scheme is seen to be marginally best across

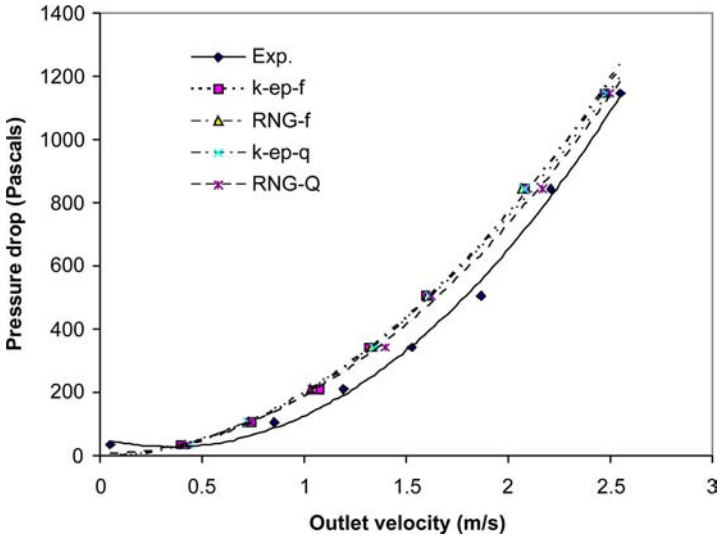

Figure 7.
Comparison of the first order upwind and the QUICK scheme using the standard k-ε and the RNG k-ε

the pressure drop range. It is interesting that the standard k-ε model with the QUICK scheme almost overlaps the RNG k-ε model with the first order scheme.

Theoretically, the RNG k-ε model was developed with more rigor and mathematical formalism based on the RNG theory. Thus, the RNG model appears to be more responsive to the changes in the complex flow structure. In the RNG k-ε model two shortcomings of the standard k-ε model were remedied by modifying the coefficients C_2 in Equation (2) and the eddy viscosity. In comparison with the k-ε model, there is smaller destruction of ε in Equation (2) for the RNG model. This larger ε gives smaller k in Equation (1). Thus, compared to the standard k-ε model, the RNG model resulted in a lower turbulence viscosity according to Equation (3), and hence higher outlet velocities. Analytis (2003) also confirmed that the RNG model increased the dissipation rate and hence, decreased the level of turbulence. However, it can be seen that it is still not sufficient for the current complex curvature correction. There are under-predictions of up to 15 per cent compared to the experimental data in the RNG model. Wang *et al.* (2006) pointed out that the proper modification of the coefficients C_2 and the eddy viscosity can improve accuracy further. This is consistent with Menter's results. Menter (1996) indicated that for the self-similar adverse pressure gradient flow, the RNG and the standard k-ε model did not predict enough retardation. They also did not reproduce backward facing step flows.

Figure 8 shows predictions from the standard two-equation k-ε model, the RNG k-ε model and the RSM all using the QUICK scheme. The RNG k-ε model and RSM give very similar results and improved prediction slightly compared to the k-ε model.

The standard k-ε model converged much quicker than the RSM and the RNG k-ε model, so the three are more comparable when computational economy is also taken into account. One possible explanation is that the difficulties experienced with the standard k-ε model in terms of predictive weaknesses and also numerical difficulties arising from the viscosity-affected near-wall properties of the ε-equation, have been improved by using the two layer near wall models. Moreover, the superposition of the complex flow phenomena, such as flow separation, accelerated, impingement and recirculation, which are incorrectly predicted by the standard k-ε models, results in a compensation. Guo *et al.* (2001) and Sarkar *et al.* (1997) showed that the k-ε model has a

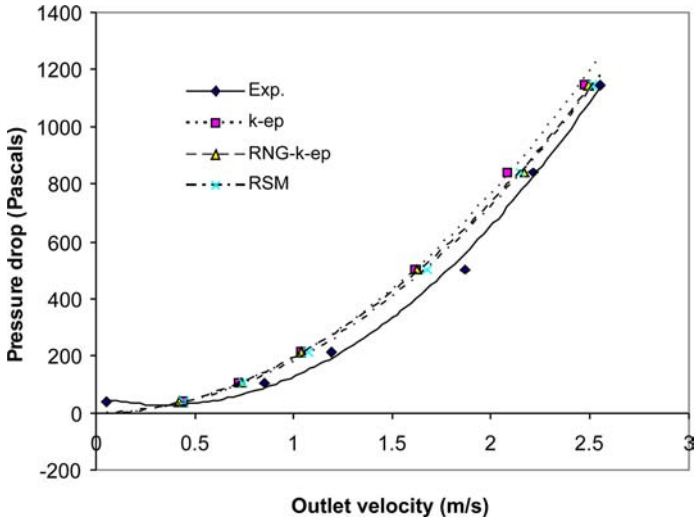

Figure 8.
Comparison of the standard k-ε, the RNG k-ε and the RSM model with the QUICK scheme

comparable behaviour to the RSM in their cases. Leschziner (2006) indicated that there is ample evidence that eddy-viscosity models, unless modified in particular non-general ways, often perform poorly in flows featuring separation, strong shock/boundary-layer interaction and 3D vertical structures. Hence, in view of the comparison between the observed and predicted behaviour, as well as the computational economy, the RSM and the RNG have no more advantage than the standard k-ε one.

6.4 Flow field analysis

The predicted velocity vectors of the eight-port STuVA using the RNG k-ε model with two layer near-wall treatment are shown in Figure 9. The fluids from the eight inlets flow through the eight narrow gaps into the vortex chamber. Every pair of inlet flows impinge on each other in the vortex chamber to form a jet. Note that the flow appears equally distributed around the periphery, with no evidence of mal-distribution of biasing. The four jets impinge in the centre of the vortex chamber and merge into the nozzle port, with some recirculation being produced. The recirculation velocity gradually increases and the area of the impingement increases with increasing inlet pressure. As expected the flow velocity is strongly accelerated in the nozzle port, with the maximum velocity at the centre of the nozzle. After the flow exits from the nozzle port, the wall bounded jet is expanded in the expanded pipe. As the inlet pressures increase the vortex of the recirculation flow in the expanded pipe moves toward the outlet. It should be mentioned that no obvious difference was found between the flow fields for the standard k-ε model, the RNG k-ε model and the RSM with the QUICK scheme.

The contours of turbulent kinetic energy are shown in Figure 10. It can be seen that there is a highest turbulent kinetic energy through the nozzle port. After enter the expansion pipe, the turbulent kinetic energy is quickly dissipated and the static pressure recovered.

The result presented here are somewhat limited against the overall pressure drop and average outlet velocity, and this can not be extended automatically to assess the performance of turbulence models for other complex geometries. Nevertheless, to some

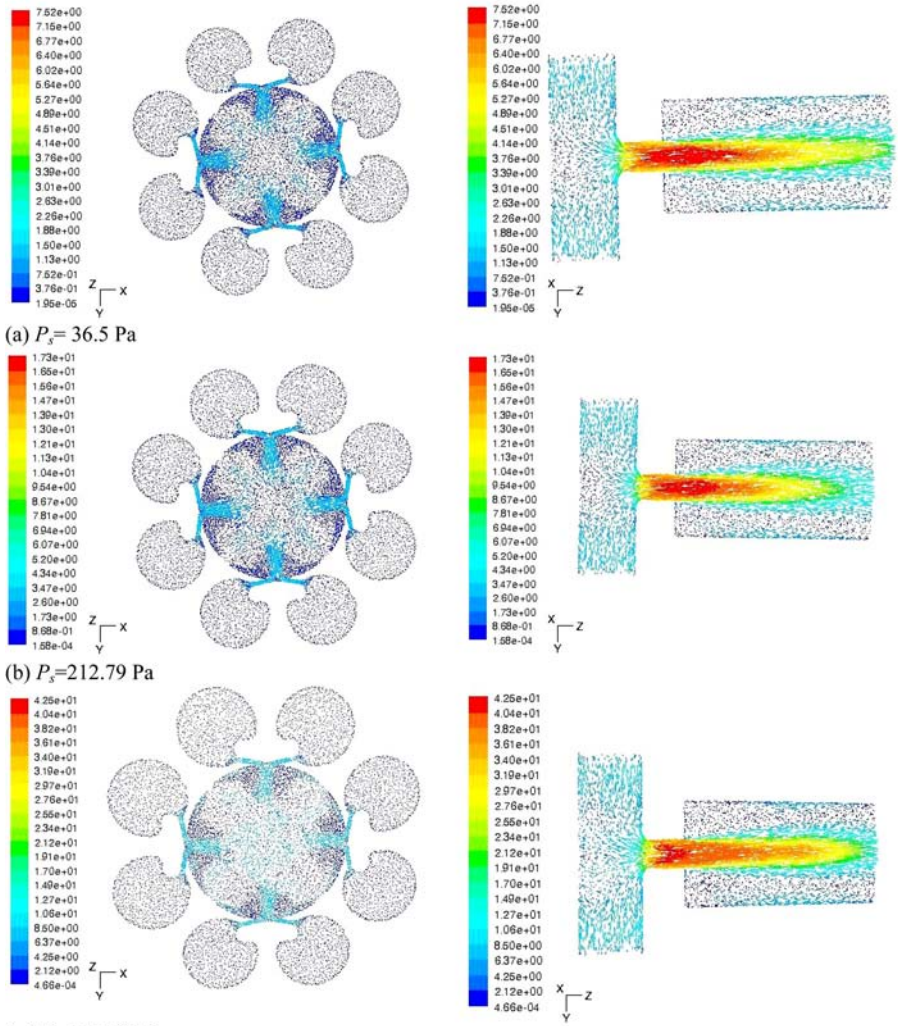

Figure 9.
Velocity vectors of the eight-port STuVA using the RNG k-ε model with the QUICK scheme and the two layer near-wall model: (a) P_s = 36.5 Pa, (b) P_s = 212.8 Pa, (c) P_s = 1,145.03 Pa

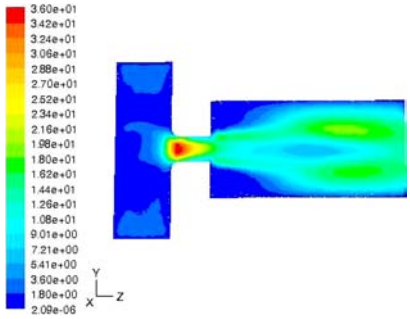

Figure 10.
Contours of the turbulent kinetic energy of STuVA

extent, they show that the theoretically higher fidelity models maybe be far from the theoretical expectation for the complex geometries. It can be served as a reference for other similar CFD simulation. The testing and improvement of the turbulence models and near wall models have been a continuous effort over the near future and more work have to be done.

7. Conclusions

Three turbulence models, the standard k-ε, the RNG k-ε and the RSM have been used to simulate numerically the confined turbulent flow in the eight-port STuVA. All the computations were performed with the same boundary conditions. The effect of different unstructured tetrahedral grids was evaluated with two discretization schemes. Numerical results show that the inlet pressure strongly affects the flow field in the STuVA. The recirculation zones in the vortex chamber and the nozzle increase as the inlet pressure increases. It is also found that the pressure drop across the vortex amplifier occurs mainly through the nozzle port. After the nozzle port, the turbulent kinetic energy dissipates quickly.

Three near wall treatments have been evaluated against the experimental data. It is shown that the near wall treatments are important when strong streamline curvature exists. The two layer near wall treatment is in better agreement with experimental data compared to the standard wall function.

The RSM gave predictions slightly closer to the experimental data than the other models, although the RNG k-ε model predicted nearly as accurately as the RSM. They both improved errors by about 3 per cent compared to the standard k-ε model but took a long time for convergence. Hence, computational economy is taken into account, the standard k-ε model is still comparable. Furthermore, the modelling of complex flows depends not only on the turbulence model but also on the near-wall treatments. In this study a good combination was the RSM, two layer wall model and the QUICK scheme, which improved accuracy by more than 10 per cent compared to the standard k-ε model, the standard wall function and first order upwind. The predicted flow fields for the eight inlet port STuVA showed no evidence of any mal-distribution of flow between the inlet ports or within the chamber, which has been noted to cause flow instabilities in simpler two port STuVA designs. This studies does give us an insight of flow fields for further design improvement of the STuVA.

References

Analytis, G.Th. (2003), "Implementation of the renormalization group (RNG) k-ε turbulence model in GOTHIC/6.lb: solution methods and assessment", *Annals of Nuclear Energy*, Vol. 30 No. 3, pp. 349-87.

Chen, H.C. and Patel, V.C. (1988), "Near-wall turbulence models for complex flows including separation", *AIAA Journal*, Vol. 26 No. 6, pp. 641-8.

Ferziger, J.H. and Peric, M. (1999), *Computational Methods for Fluid Dynamics*, 2nd edition, Springer-Verlag, Berlin.

Guo, B., Langrish, T.A.G. and Fletcher, D.F. (2001), "An assessment of turbulence models applied to the simulation of a two-dimensional submerged jet", *Applied Mathematical Modelling*, Vol. 25, pp. 635-53.

He, P., Salcudean, M. and Gartshore, I.S. (1999), "A numerical simulation of hydrocyclones", *Transactions of the Institution of Chemical Engineers, Part A*, Vol. 77, pp. 429-41.

Johston, J.P. and Flack, K.A. (1996), "Review – advances in three dimensional turbulent boundary layers with emphasis on the wall-layer regions", *ASME Journal of Fluids Engineering*, Vol. 118, pp. 219-32.

Launder, B.E. and Spalding, D.B. (1974), "The numerical computation of turbulent flows", *Computer Methods in Applied Mechanics and Engineering*, Vol. 3, pp. 269-89.

Leschziner, M.A. (2006), "Modelling turbulent separated flow in the context of aerodynamic applications", *Fluid Dynamics Research*, Vol. 38 Nos. 2-3, pp. 174-210.

Malhotra, A., Branion, R.M.R. and Hauptmann, E.G. (1994), "Modelling the flow in a hydrocyclone", *Canadian Journal of Chemical Engineering*, Vol. 72, pp. 953-60.

Menter, F.R. (1996), "A comparison of some recent eddy-viscosity turbulence models", *ASME Journal of Fluid Engineering*, Vol. 118, pp. 514-19.

Patankar, S.V. and Spalding, D.B. (1972), "A calculation procedure for heat, mass and momentum transfer in three-dimensional parabolic flows", *International Journal of Heat and Mass Transfer*, Vol. 15 No. 10, pp. 1787-806.

Patel, V.C., Rodi, W. and Scheuerer, G. (1985), "Turbulence models for near-wall and low Reynolds number flows: a review", *AIAA Journal*, Vol. 23 No. 9, pp. 1308-19.

Priestman, G.H. and Tippetts, J.R. (1984), "Development and potential of power fluidics for process flow control", *Transactions of the Institution of Chemical Engineers, Part A*, Vol. 62 No. 2, pp. 67-80.

Priestman, G.H. and Tippetts, J.R. (1998), "The application of power fluidics to level control in multiphase separators", *Proc Symp "Multiphase Technology", BHR Group, Cranfield*, pp. 119-29.

Priestman, G.H. and Tippetts, J.R. (2000), "Fluidic level control in gas–liquid separators", *Transactions of the Institution of Chemical Engineers, Part A*, Vol. 78 No. A5, pp. 690-7.

Sarkar, T., Sayer, P.G. and Fraser, S.M. (1997), "Flow simulation past axisymmetric bodies using four different turbulence models", *Applied Mathematical Modelling*, Vol. 21 No. 12, pp. 783-92.

Slack, M.D., Prasad, R.O., Bakker, A. and Boysan, F. (2000), "Advances in cyclone modelling using unstructured grids", *Transactions of the Institution of Chemical Engineers, Part A*, Vol. 78, pp. 1098-104.

Thakur, S., Wright, J., Shyy, W., Liu, J., Ouyang, H. and Vu, T. (1996), "Development of pressure-based composite multigrid methods for complex fluid flows", *Progress in Aerospace Sciences*, Vol. 32, pp. 313-75.

Versteeg, H.K. and Malalasekera, W. (1995), *An Introduction to Computational Fluid Dynamics: The Finite Volume Method*, Longman Scientific & Technical, London.

Wang, H., Beck, S.B.M., Priestman, G.H. and Boucher, R.F. (1997), "Fluidic pressure pulse transmitting flowmeter", *Transactions of the Institution of Chemical Engineers, Part A*, Vol. 75 No. A4, pp. 381-91.

Wang, J.Y., Priestman, G.H. and Tippetts, J.R. (2006), "Modelling of strongly swirling flows in a complex geometry using unstructured meshes", *International Journal of Numerical Methods for Heat and Fluid Flow*, Vol. 16 No. 8, pp. 910-26.

Wolfstein, M. (1969), "The velocity and temperature distribution of one-dimensional flow with turbulence augmentation and pressure gradient", *International Journal of Heat and Mass Transfer*, Vol. 12, pp. 301-18.

Woolhouse, R.J., Tippetts, J.R. and Beck, S.B.M. (2000), "A comparison of the experimental and computational modelling of the fluidic turn-up vortex amplifier at full and zero swirl conditions", *Proceedings of Institute of Mechanical Engineers, Part C, J. of Mechanical Engineering Science*, Vol. 215, pp. 893-903.

Yang, Z.Y., Priestman, G.H. and Boysan, H.F. (1991), "Internal flow modelling of vortex throttles", *Proceedings of Institute of Mechanical Engineers, Part C, Journal of Mechanical Engineering Science*, Vol. 205, pp. 405-13.

Younis, B.A., Gatski, T.B. and Speziale, C.G. (1996), "Assessment of the SSG pressure-strain model in free turbulent jets with and without swirl", *ASME Journal of Fluid Engineering*, Vol. 118 No. 4, pp. 800-9.

Further reading

FLUENT Incorporated (n.d.), *FLUENT6.2.16 User's Guide*, online version.

Corresponding author

Junye Wang can be contacted at: junye.wang@bbsrc.ac.uk